JGR Planets

RESEARCH ARTICLE
10.1029/2022JE007438

Surface Energy Fluxes and Temperatures at Jezero Crater, Mars

H. I. Savijärvi[1,2], **G. M. Martinez**[3,4], **and A.-M. Harri**[2]

[1]Institute for Atmospheric and Earth System Research/Physics, University of Helsinki, Helsinki, Finland, [2]Finnish Meteorological Institute, Helsinki, Finland, [3]Lunar and Planetary Institute, Universities Space Research Association, Houston, TX, USA, [4]Department of Climate and Space Sciences and Engineering, University of Michigan, Ann Arbor, MI, USA

Abstract Diurnal ground surface and air temperatures (T_g, T_a) and the five major surface energy budget fluxes are displayed as derived from M2020 mission observations and from column model simulations in two extreme cases (low and high diurnal T_g-variation) along the Perseverance rover track in the Jezero crater. In both cases the fluxes and T_g are well modeled when using diurnally variable apparent ground thermal inertia I derived via a Fourier series method from the hourly observations. Hence the measurements, the diagnostic method and the model results are consistent with high- and low-I nonhomogeneous terrain in the field-of-view (FOV) of the thermal infrared and solar sensors. In contrast less extreme values of I consistent with THEMIS retrievals are necessary for good simulations of observed T_a. We deduce that the measured T_g for the small ∼3 m^2 FOV may not always be representative for the larger region around the rover, which controls the near-surface atmospheric temperature profile.

Plain Language Summary We present comparisons of hourly surface and air temperatures and solar and thermal (atmospheric) radiation as measured by Perseverance during quite low and quite high noon temperature. We also compare the observed values to those produced by a numerical model. It appears that the model can produce excellent simulations of radiation and the ground surface temperature, if the small measurement spot for the latter is assumed to be a thermally extreme and nonhomogeneous mixture of sand and rocks (models usually assume homogeneous ground). Less extreme soil properties, such as measured by satellites, are needed instead for good air temperature predictions at 1.5 m height, as air temperatures are controlled by larger areas of surface temperatures around the rover. These results are important to better interpret local measurements by Perseverance and to provide ground-truth to satellite observations with a much greater spatial resolution.

1. Introduction

The M2020 mission rover "Perseverance" landed onto the Jezero crater of Mars (18.36°N, 77.59°E) in February 2021 at the beginning of local northern hemisphere spring. Perseverance is equipped with the Mars Environmental Dynamics Analyzer (MEDA, Rodriguez-Manfredi et al., 2021). MEDA measures, among other quantities, four surface radiative fluxes and the ground surface temperature (T_g) via thermal infrared and solar sensors (MEDA TIRS; Sebastián et al., 2021; Sebastián et al., 2020; Perez-Izquierdo et al., 2018). Air temperatures at about 1.45 m height (T_a) are measured by three MEDA Air Temperature Sensors (ATS 1–3) and by the humidity sensor (MEDA HS), all located around the remote sensing mast to minimize thermal influence from the rover. Based mainly on these measurements and column modeling we present initial results for the diurnal energy exchanges at the Martian surface along Perseverance's traverse. We concentrate here on two contrasting early-summer periods, during which the rover was stationary.

At any time energy is conserved at the ground surface of Mars. Hence the surface energy budget (SEB) can be written as follows:

$$G = \text{SWD} - \text{SWU} + \text{LWD} - \text{LWU} - \text{TF} - \text{LF} \tag{1}$$

here G is the net heat flux into the ground, SWD the downwelling shortwave (solar) radiation transmitted through the atmosphere, SWU the upwelling solar radiation reflected by the ground, LWD the downwelling longwave (thermal infrared, IR) radiation emitted by the overlaying atmosphere, LWU the upwelling longwave radiation emitted by the ground surface, TF the sensible heat flux associated with turbulent motions and LF the latent heat

Special Section:
The Mars Perseverance Rover Jezero Crater Floor Campaign

Key Points:

- MEDA-observed radiative fluxes and ground temperatures T_g are compared to model simulations during weak and strong diurnal variation in T_g
- Radiation and T_g are best modeled with use of diurnally variable apparent thermal inertias
- Air temperatures are best modeled with less extreme area-averaged thermal inertias

Correspondence to:
H. I. Savijärvi,
hannu.savijarvi@helsinki.fi;
hisavijarvi@gmail.com

Citation:
Savijärvi, H. I., Martinez, G. M., & Harri, A.-M. (2023). Surface energy fluxes and temperatures at Jezero crater, Mars. *Journal of Geophysical Research: Planets*, *128*, e2022JE007438. https://doi.org/10.1029/2022JE007438

Received 22 JUN 2022
Accepted 14 NOV 2022

Author Contributions:
Conceptualization: H. I. Savijärvi
Data curation: G. M. Martinez, A.-M. Harri
Formal analysis: H. I. Savijärvi, G. M. Martinez
Funding acquisition: A.-M. Harri
Investigation: H. I. Savijärvi, G. M. Martinez
Methodology: H. I. Savijärvi, G. M. Martinez
Project Administration: A.-M. Harri
Software: H. I. Savijärvi
Supervision: H. I. Savijärvi, A.-M. Harri
Validation: H. I. Savijärvi, G. M. Martinez
Visualization: H. I. Savijärvi, G. M. Martinez
Writing – original draft: H. I. Savijärvi
Writing – review & editing: G. M. Martinez, A.-M. Harri

flux associated with moisture exchanges at the surface. Martinez et al. (2021) displayed hourly values of the SEB fluxes from the first 2,500 solar day (sol) data of the Mars Science Laboratory (MSL) mission on the Gale crater at 4.6°S, the LWD there not measured, but derived as the residual in Equation (1). In the M2020 mission LWD as well as SWD, SWU, and LWU are directly measured by the MEDA TIRS device, providing novel in situ flux validation data for atmospheric models.

The MEDA observation-based hourly T_g, T_a, and the above four radiative fluxes are here displayed and results from the University of Helsinki/Finnish Meteorological Institute Single-Column Model (SCM) are compared to them in two extreme cases. Our aim is to reveal possible deficiencies in the model and to interpret the observations. Our first case at Jezero is characterized by a particularly small diurnal variation in observed T_g and a curious lack of a typical nocturnal temperature inversion in the observations. The second period displays instead quite a large diurnal range in T_g with a strong observed inversion. A diagnostic method to derive a diurnally varying soil thermal inertia from the observations is presented. Use of it improves the diurnal simulation of T_g in both cases and leads to an explanation for the lack of inversion.

The methods, the model and data selection are briefly described in Section 2. Then the ground and air temperatures and the energy budgets during the two periods are considered in Sections 3–5, respectively. Discussion is in Section 6 and our conclusions are given in Section 7.

2. Methods, Model, and Data Selection

Values of the daytime dust visual opacity τ_{vis} (derived from the MastCam-Z instrument), the mean surface pressure p, noon albedo α and the hourly values of T_g, T_a, and the surface radiative fluxes of Equation (1) are here obtained from the M2020 mission observations as presented with their error bars in Martínez et al. (2023). G can then be estimated from Equation (1) as the observed radiation balance, by discarding the small TF (a few % of G) and the tiny LF (<0.1 Wm^{-2}).

G may also be obtained, as in Savijärvi, Martinez, Vicente-Retortillo, and Harri (2022) and Savijärvi, Martinez, and Harri (2022), by first Fourier analyzing the diurnal cycle of hourly T_g. For hour $h = 0, 1, 2, \ldots, 23$ the nonaliased Fourier series of $T_g(h)$

$$T_g(h) = T_m + \Sigma_{n=1}^{10}(A_n \, sin(x) + B_n \, cos(x))$$

(where T_m is the diurnal mean and $x = n \times 2\pi h/24$) reproduces the observed hourly values typically within ±0.1 K at any sol. Each Fourier wave $T_{gn}(t)$ as the top boundary condition forces in the linear soil thermal diffusion equation (with constant thermal conductivity λ, volume heat capacity ρc and thermal inertia $I = (\lambda\rho c)^{1/2}$) a known damped and delayed wave solution $T_n(t,z)$ into the soil. Setting these to $G = -\lambda(\delta T/\delta z)_{z=0}$ leads via analytic differentiation and summing to:

$$G(h) = I \cdot \Sigma_{n=1}^{10}[C_n(A_n(\sin(x) + \cos(x)) + B_n(\cos - \sin(x)))] = I \cdot S(h) \quad (2)$$

where $C_n = (n.\pi/D)^{1/2}$, $D = 88{,}775$ s (Mars sol length), and $S(h)$ is the sum in Equation 2. For constant thermal inertia I the resulting $G(h)$ is similar to a high-resolution numerical solution to the same problem (such as e.g., in Martinez et al., 2021). A benefit of Equation 2 is that approximate hourly values for apparent I can now be obtained by substituting Equation 2 into Equation 1, and then solving for $I(h)$; $I(h) = (\text{SWD} - \text{SWU} + \text{LWD} - \text{LWU})/S(h)$ (thus discarding the small TF and LF) and inserting the four observed hourly radiation fluxes. The resulting data-based diurnally variable values for apparent $I(h)$ are associated with changes in $G(t)$ as the thermal wave propagates down into inhomogeneous soil. These diagnostic values of $I(h)$ may be compared with the physical-computational results of Putzig and Mellon (2007) for apparent $I(h)$ in horizontally inhomogeneous soil. The variable $I(h)$ can also be used in models by interpolating linearly between the hourly values of I at each time step. Here we limit $I(h)$ to 0.3…1.3 of the respective constant I for each sol, as near-zero values of $G(h)$ and S(h) in midmorning and midafternoon may lead to arbitrary values of $I(h)$.

Our University of Helsinki/Finnish Meteorological Institute adsorptive SCM is a hydrostatic model without advections, forced by geostrophic wind (here 10 m/s) and varying T_g. With surface roughness length of 1 cm it provides here winds at 1.5 m of ~5 ms^{-1} at daytime and ~1.5 ms^{-1} at night, in line with measurements from MEDA's wind sensor (Newman et al., 2022). Parameterizations for radiation, moist physics and

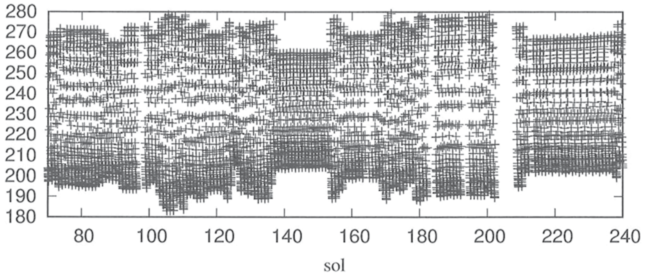

Figure 1. MEDA-observed surface temperatures T_g (K) for sols 75–240. Note a low diurnal variation during sols 138–152, and a high variation at sols 181–199. The rover was stationary during these two periods.

the stability- and wind-dependent local turbulence produce the model's six right-hand-side fluxes of Equation 1, the sum-G then driving soil thermal diffusion in eight soil points at optimized nondimensional depths (Savijärvi & Määttänen, 2010; Savijärvi et al., 2016). There are 29 air grid points up to 40 km height, the lowest being at 0.3, 0.7, and 1.45 m heights. Solar radiation takes into account CO_2 and dust via a modified delta-two-stream scheme with dust single-scattering albedo of 0.90 and asymmetry parameter of 0.70 (Chen-Chen et al., 2021; Savijärvi et al., 2005). Local slope effects on SWD are included as in Savijärvi, Martinez, Vicente-Retortillo, and Harri (2022) and Savijärvi, Martinez, and Harri (2022) using the current yaw, pitch and roll of the rover. Thermal radiation is calculated via a fast emissivity method for CO_2, H_2O and dust, with the dust-τ_{vis}/τ_{IR} ratio optimized to 2.0 for the upwelling, 4.0 for the downwelling LW fluxes at each height (Savijärvi et al., 2020).

The model is initialized from a realistic temperature profile with dust and moisture vertically well-mixed. It is then run to sol 3, whereby it has spun up to a repeating diurnal cycle of temperatures, winds and moistures. These sol-3 values are then compared with the observation-based values, the model's quoted accuracy based later on mostly on fits by eye based on the figures. Moistures are not discussed here as LF is insignificantly small in the present cases (model-LF < 0.1 Wm^{-2}). Thus LF has no practical impact on T_g through Equation 1. Initial MEDA moisture measurements and SCM simulations are presented in Polkko et al. (2023).

Figure 1 shows observed T_g for sols 75–240. A particularly low diurnal variation in T_g is seen at sols 138–152, and a high variation at sols 181–199. The rover was stationary during these periods, the first period being near aphelion (L_s 71°) and the second near the northern summer solstice (L_s 90°). The two locations along the Perseverance track are marked to Figure 2, which also displays thermal inertias estimated from THEMIS retrievals in ~100 m × 100 m resolution in the Jezero area. The THEMIS inertias appear to be typically in the range of 300–400 J m^{-2} K^{-1} s$^{-1/2}$ (SI units, units omitted hereafter) along the rover track.

3. Results: Sol 143; Low Diurnal Variation in Observed T_g

During sols 138–152 (L_s 70°–76°) the rover was stationary with mean observed surface pressure p being about 7.5 mb, τ_{vis} about 0.40 and noon albedo α about 0.14. Figure 3 displays the MEDA-observed values of T_g during sol 143 (stars), the other sols being very similar (Figure 1). The indicated accuracy for T_g is here from ±0.37 K at midnight to ±0.45 K at midday. Shown are also three SCM simulations for L_s of 72° (lines) with the above observed p, τ_{vis}, and α. The simulation with a constant high thermal inertia I of 600 (thick dashes) reproduces the observed minima and maxima of T_g and the phase fairly well. However, it displays a moderate cold bias of 5–7 K during midmorning. The simulation with a lower THEMIS-indicated I of 350 (dots) shows a large difference to the T_g -data, with a cold night-time bias of 10 K and a warm bias at noon of 17 K; it is shown here for comparison and for later reference. The simulation with a diurnally variable apparent I (thin solid line) is instead nonbiased at all hours. This will be commented below.

Figure 4 shows the measured diurnal SEB for sol 143. It displays the four novel MEDA-observed radiation fluxes and G as the radiation balance (symbols). Shown are also the same fluxes from the SCM simulation with the variable I (thin solid lines). All four radiation fluxes appear to be quite well simulated. Largest discrepancies occur in SWD (and hence also in G) near sunrise and sunset. LWD is smooth and small. The observed radiation fluxes and model results are nearly identical also during the other sols of the period. The good match of the observed and modeled SWD and LWD means that the model's internal parameters and its fast broadband methods are adequate in representing the complex scattering, absorption and emission of airborne dust.

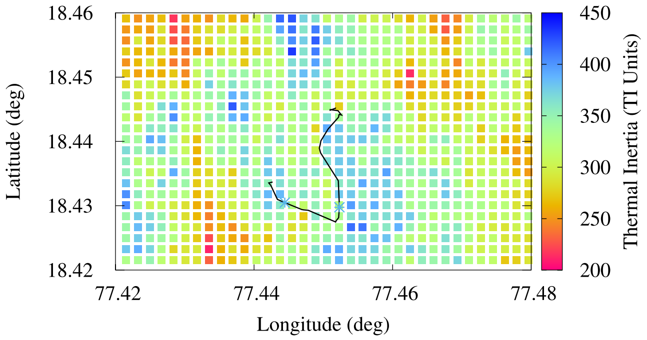

Figure 2. Perseverance track and thermal inertia values I (J m^{-2} K^{-1} s$^{-1/2}$) as retrieved from THEMIS. The eastern star is at sols 138–152, the western at sols 181–199, with I at both sites ~350 SI units.

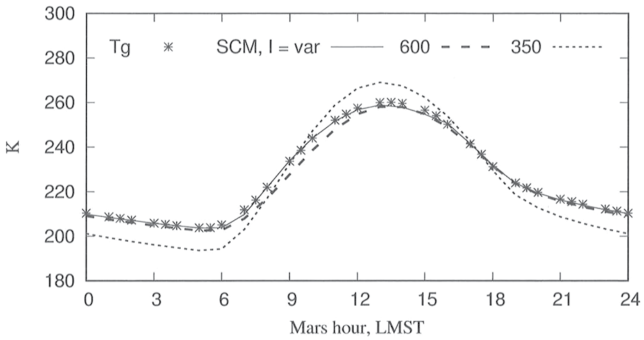

Figure 3. MEDA-observed T_g for sol 143 (symbols), and T_g from SCM simulations (lines) for ground thermal inertia I of 600 and 350 SI units, and for the diurnally variable apparent I (I = var, from Figure 5). The I = var simulation (thin line) is good, the $I = 600$ simulation shows a cold bias during the morning hours. The $I = 350$ simulations is not so good for T_g.

Dashed line in Figure 4 is the turbulent sensible heat flux (TF) from the simulation. It is small (because of small density of air), only about 12 Wm^{-2} during the highly convective midday, and around -1 Wm^{-2} during the stable and calm night. Hence G as a radiation balance is here a good approximation. When this is applied to get the apparent hourly $I(h)$ from the data via the Fourier T_g-method described in Section 2, the result is Figure 5. Here I is about 600 during late evening and night but drops suddenly to below 300 after sunrise; then increases to about 700 by 15:00 local mean solar time (LMST), dropping again temporarily at 16:00 LMST. Similar behavior of apparent $I(h)$ was seen in Putzig and Mellon's (2007) experiments for horizontal mixtures of low-I and high-I soil. The physical explanation is that after sunrise the low-I materials of the top regolith (*e.g.*, fine sands and dust) warm up very rapidly in the increasing sunshine, dominating in apparent I, whereas the high-I materials (rocks, bedrock) warm up more slowly, dominating the apparent I in the early afternoon. Likewise, when G turns negative at about 16:00 LMST (Figure 3), the low-I fractions begin to cool down rapidly, leading temporarily to a low apparent I, the slower and warmer high-I materials dominating the apparent I later on. The average I in Figure 5 (dashed line) is 562, not far from the constant value of 600, which produced a good T_g-simulation in Figure 3, although with a cold bias of $\sim$5 K in midmorning as an indication of too high I.

When this diagnostic apparent $I(h)$ (thin line of Figure 5) is used in the simulation, a good match with the observed T_g is obtained (thin line in Figure 3). In particular the cold morning bias of the constant-I simulation is gone. The heterogeneous regolith in the field-of-view of the MEDA-TIRS sensors for T_g and LWU thus appears to consist here mainly of high-I bedrock, with some contribution from fine sands. Such a mixture explains the diurnal variation of the apparent thermal inertia and also the cold morning bias in the constant-inertia T_g-simulation. Figure 6 reveals that the small $\sim$3 m^2 area of the TIRS downscan indeed consists here mainly of fractured bedrock slabs, with sand in between. However, this high-I bedrock-dominated spot may not represent the typical ground around the rover, as can clearly be seen in Figure 6. This is discussed further in the next section.

4. Air Temperatures on Sol 143

Figure 7 shows the hourly air temperatures (T_a) for sol 143 as measured by ATS1, ATS2, ATS3, and HS at about 1.45 m height (The ATS1-5 and HS observations are described and discussed in detail in Munguira et al. (2023) and Polkko et al. (2023)). Scatter in these observations is large during the turbulent afternoon, but together they do indicate the typical diurnal cycle of observed T_s for this sol. Figure 7 also displays T at 1.45 m from the simulation with $I = 350$ (thick line) and with the variable apparent $I(h)$ (thin line). The latter produced the good simulation for T_g in Figure 3 but here the $I = 350$ simulation (thick line) is much more consistent with observations of T_a, especially at night. Crosses in Figure 7 are the observed ground temperatures from Figure 3. They are, curiously, much warmer than the observed air temperatures during the night, whereas a strong nocturnal inversion ($T_g < T_a$) is typical for Mars, due to the strong net cooling of the ground ($G << 0$, Figure 4).

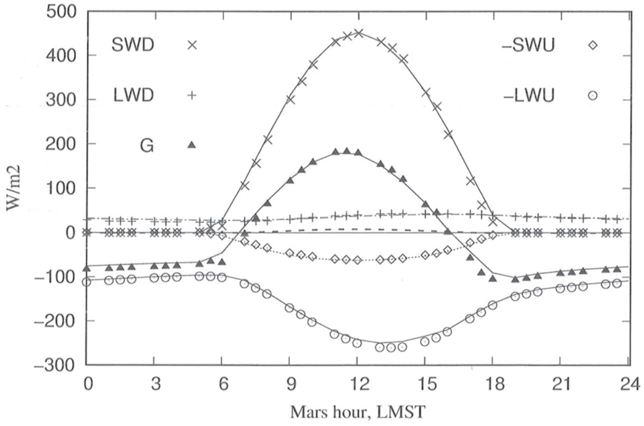

Figure 4. Surface energy fluxes from MEDA observations for sol 143 (symbols), and from the SCM simulation with the variable thermal inertia (solid lines). Dashed line is the model's turbulent sensible heat flux TF. Observed net heat flux into the ground G is estimated here as the radiation balance (G = SWD + LWD − SWU − LWU), as TF is very small.

Figure 8 concentrates on the 00:00–06:00 LMST night period, adding values of model-T_g. The $I = 350$ simulation (thick line) fits within the observed T_a fairly well and provides a typical inversion (T_g 3–4 K < T1.5 m) during the night, but its T_g (thick dashes) is much too cold compared to observed T_g. In strong contrast, the simulation with I = var (thin dashes) reproduces the T_g-observations much better and provides a typical inversion of 2–3 K, but its T_a (thin line) is much too warm compared to observed T_a.

We interpret this inversion problem as follows: The small ($\sim$3 m^2) field of view (FOV) of the TIRS downscans for T_g and LWU provides here good-quality retrievals for these variables. Hence also the model, when using

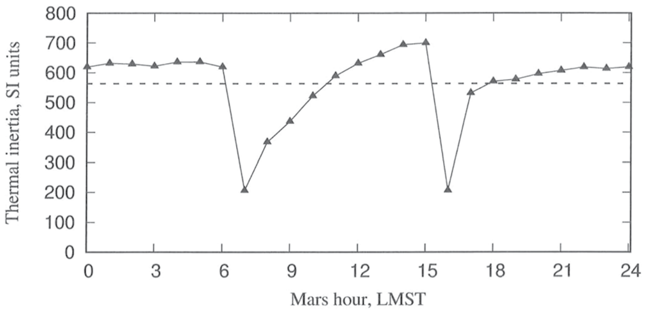

Figure 5. The hourly variable apparent thermal inertia (var-I) for sol 143 as calculated from observed T_g and the radiation balance via the Fourier method described in Section 2. This $I(h)$ produces the good SCM simulations in Figures 3 and 4. Dashed line ($I = 562$) is the diurnal mean.

constant I and $I(h)$ derived using them, is able to simulate the observed T_g fairly well. However, the small FOV landed here on a bedrock-dominated spot (Figure 6). This may not represent the typical regolith around the rover, which largely controls the air temperatures. The effective (area-averaged) I is hence better obtained here by fitting model's T_a to observed T_a, as in Figure 7, instead of fitting T_g. The resulting value, $I \sim 350$, is consistent with the large-area THEMIS estimate for this location (Figure 2).

5. Results for Sols 189; High Diurnal Variation in Observed T_g

Perseverance was stationary with consistently high and repetitive diurnal T_g-variation on sols 181–199 at L_s 89°–98° (Figure 1). The observed mean p was about 7.1 mb, τ_{vis} about 0.45 and α about 0.12. Figure 9 shows the MEDA-observed T_g on sol 189 with a high diurnal range of 191–277 K. The indicated accuracy for T_g is here from ±0.39 K at midnight to ±0.63 K at midday. Shown are also SCM simulations with the above three main parameter values for L_s 92.5°, using three thermal inertias. From these $I = 350$ slightly underestimates the observed T_g-range. Use of $I = 290$ provides here a better simulation, being however too cold in midmorning. Use of apparent variable I produces the best simulation for T_g, except at 06:00 LMST.

The measured diurnal SEB for sol 189 (Figure 10) is broadly similar to that of sol 143 (Figure 3), but G is now much lower in midmorning, as LWU is high, due to the high T_g. The model's SEB fluxes are relatively accurate, except for SWD and G at 06:00 LMST. Here the MEDA SWD sensor was not functioning at 06:00 LMST in the high-gain mode necessary to measure the low fluxes near the sunrise. Hence the observed SWD and the observation-based radiation balance G are biased at this hour, and so is the G-based apparent $I(h)$. This explains the inaccuracy of T_g at 06:00 LMST in the var-I simulation of Figure 9.

The behavior of var-I ($I(h)$, Figure 11) is here broadly similar to that in Figure 4 but the values are much smaller, the diurnal mean being 280. The $I(h)$-minima at 06:00 and 15:00 LMST and the increase from 06:00 to 14:00 LMST again indicate some heterogeneity. The quite homogeneous-looking sandy regolith in the TIRS downscan area for T_g (Figure 12, inlet) thus appears to include contributions from finer and coarser materials.

Figure 13 presents measurements of T_g and T_a for sol 189 (symbols), together with T at 1.5 m height from SCM with $I = 350$ and with the variable I (curves). The scatter in the hourly T_a-observations is again large in the convective afternoon, the $I = 350$ simulation providing a slightly better fit to the cloud of observations. Here the

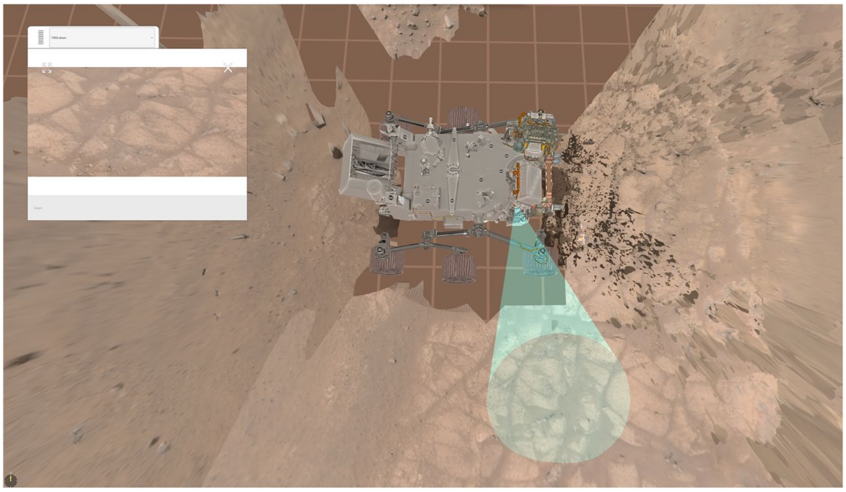

Figure 6. The ground around Perseverance on sol 143. The small field of view (~3 m^2) of the MEDA ground-viewing sensors is in the inlet. It consists mainly of exposed bedrock, whereas the site around the rover appears to be mainly of sandy regolith.

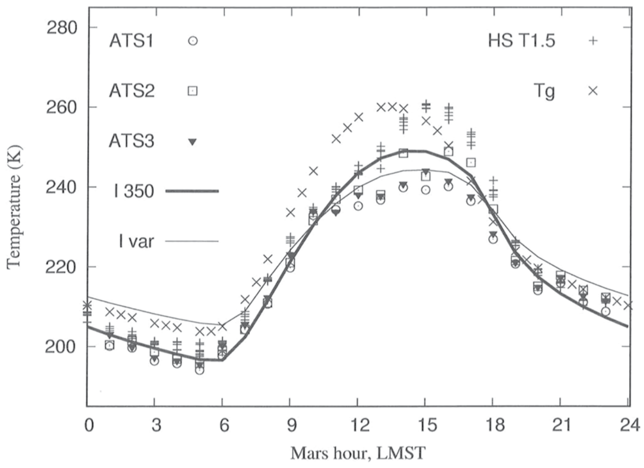

Figure 7. Air temperatures at ~1.45 m height for sol 143 from MEDA ATS and HS (symbols), and from SCM simulations (lines) for I = var (~600) and for $I = 350$. Observed T_g is also shown.

nocturnal inversion is quite strong in the observations, opposite to the sol 140–150 case. The 00:00–06:00 LMST period is enlarged into Figure 14, also including the two SCM simulations of T_g. From Figure 14 it is seen that $I = 350$ (thick lines) provides a good simulation for T_a but a bad one for T_g, and vice versa for I = var (~290, thin lines). The inversion (T_a–T_g) is weaker in the simulation with the higher I of 350, as can be expected.

This case is hence opposite to that in sols 138–152. The TIRS downscan FOV now falls on a sandy spot on the regolith next to the rover, leading to a low estimated thermal inertia of ~280 with some heterogeneity. The nocturnal inversion as based on observations of T_a and T_g is therefore slightly stronger than a typical inversion. The T_a observations suggest, by model fits, a generally higher area-average thermal inertia of ~350 for this site. This slightly higher value agrees with the THEMIS retrieval (Figure 2) for the location, which appears to be on sandy low-I regolith with scattered higher-I rocks, as seen in Figure 12.

6. Discussion

The good match between the measured and simulated values of T_g and the SEB terms suggests that (a) MEDA's measurements are robust and fairly accurate, and (b), the column model and its input and internal parameter values would also appear to be relatively accurate. Occasional mismatches might be used to check the data or the model; for instance a temporary saturation of the SWD sensor was noticeable at 06:00 LMST in Figure 10. On the other hand the sky-viewing MEDA sensors for SWD and LWD are not sensitive to the ground around the rover (except for rover slope and ground slope effects), unlike SWU, LWU and T_g, which are derived from sensors scanning a small (~3 m^2) field-of-view area of the ground about 4 m away from the rover (Rodriguez-Manfredi et al., 2021).

Hourly values for apparent thermal inertia $I(h)$ could here be estimated from the hourly measurements of the radiation fluxes and T_g via the diagnostic Fourier method described in Section 2. Diurnally varying values of I indicate inhomogeneity in the ground (Putzig & Mellon, 2007). Hence this method can be used to chart the ground heterogeneity in the FOV area for any sol, where the rover is stationary, by using solely the hourly MEDA observations along the Perseverance track.

Use of these hourly thermal inertias in the model then led to improved predictions for T_g, thus mutually validating the MEDA measurements, the Fourier method, the resulting values of $I(h)$, and the model. In particular, the cold morning bias, which has plagued constant-I simulations of T_g (*e.g.*, Hamilton et al., 2014; Vasavada et al., 2017) then disappears, as was already shown for some MSL cases in Savijärvi, Martinez, Vicente-Retortillo, and Harri (2022) and Savijärvi, Martinez, and Harri (2022). Hence a systematic cold morning bias in T_g (or T_a) in any model simulation, which uses a diurnally constant I, could alternatively be used to indicate the degree of heterogeneity of the ground, if the Fourier method cannot be applied.

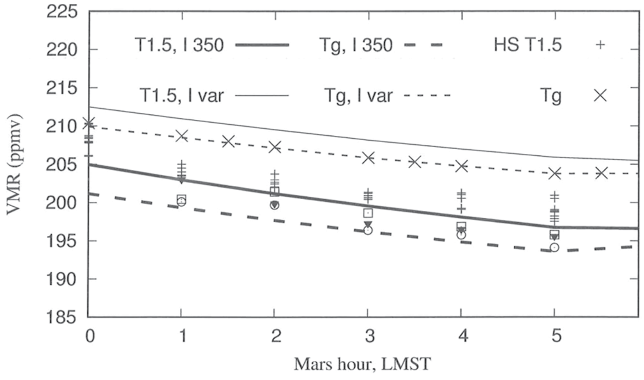

Figure 8. The nocturnal 00:00–00:06 LMST period of Figure 7 enlarged, with simulated T_g (dashed) added. The two SCM simulations indicate a typical inversion, $I = 350$ better matching with the measurements of air-T, and I = var with those of T_g. Observed values do not indicate any inversion.

A more physical way to represent the heterogeneity and to study the properties of the soil would be to use a tile method in the model (combining soil columns of e.g., sand and rock, as e.g., in Putzig and Mellon (2007) and Vasavada et al. (2017)). The diagnostic values of $I(h)$ may be of guidance for that. This is left for future, as the SCM is not yet equipped for the tile method.

However, the small TIRS field of view of the ground may not always represent the typical soil around the rover, which controls the area-averaged T_g and thereby the air temperatures. This became clear in comparing here the two extreme cases of low and high diurnal T_g-variation. The derived I-values were, respectively, around 600 and 280, producing good simulations for T_g. Instead, thermal inertia had to be about 350, in both cases, for good simulations of the respective observed *air* temperatures T_a. These less extreme I-values are close to those obtained for the respective sites by the orbit-based THEMIS

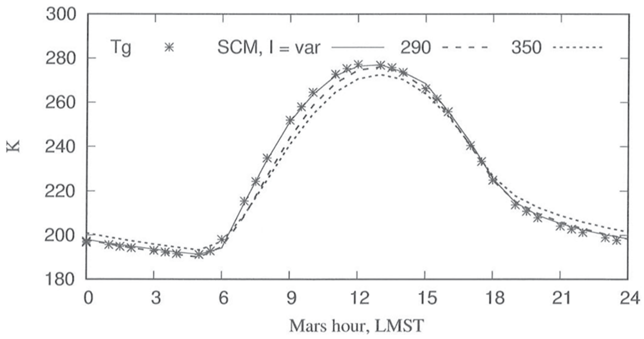

Figure 9. Observed T_g for sol 189 (symbols), and T_g from SCM simulations (lines) for ground thermal inertia I of 290 and 350 SI units, and for the diurnally variable apparent I of Figure 11.

retrievals. Hence, if an effective ("average") local value for the ground thermal inertia is needed from lander data, this should be estimated rather by model fits to observed air temperatures (as done in Figures 7 and 13) than by fits to observed T_g.

The small FOV may also explain at least partly the nocturnal inversion problems in the MEDA data. In our case of low diurnal T_g-range (indicating high *I*), the observed T_g was *warmer* than observed T_a during the night (hence no inversion!). In such cases the small FOV may lie mainly on exposed bedrock of high *I*; possibly not representative of the overall *I* of the environment that determines T_a. Thus T_g could be relatively high at night on such a spot and much higher than in the rapidly cooling sandy environment.

In our opposite case of high diurnal T_g-range the observation-based nocturnal inversion was even stronger than expected. The FOV was located here on a sandy low-*I* portion of the regolith. The small FOV is thus both a blessing and a curse: it provides for quite accurate ground measurements, but these may only represent the small FOV area and may not hold more generally.

7. Summary and Concluding Remarks

We displayed here the diurnal MEDA-observed ground and air temperatures and the measured SEB fluxes during two contrasting periods along the Perseverance track in the Jezero crater, and compared the UH/FMI SCM predictions to them. The periods were characterized by particularly low and high ranges in diurnal T_g, the rover being stationary.

The low-range period (T_g 204–260 K) was on sols 138–152 (L_s 70°–76°). Here T_g and the SEB fluxes were moderately well simulated, albeit T_g with a cold morning bias, when using a high constant thermal inertia *I* of 600 for the ground. A better nonbiased simulation for T_g was obtained when using observation-based hourly values for apparent *I*(*h*) from a diagnostic Fourier series method described in Section 2. In strong contrast, for near-accurate simulations of the measured air temperatures T_a at ~1.5 m height, a much lower *I* of 350 (*i.e.*, values of *I* typical of the large-scale environment as observed from orbit) was necessary instead. The model's nocturnal inversion (T_g 3–4 K < T_a) was then typical for Mars, whereas there was no inversion at all in the observed T_g and T_a.

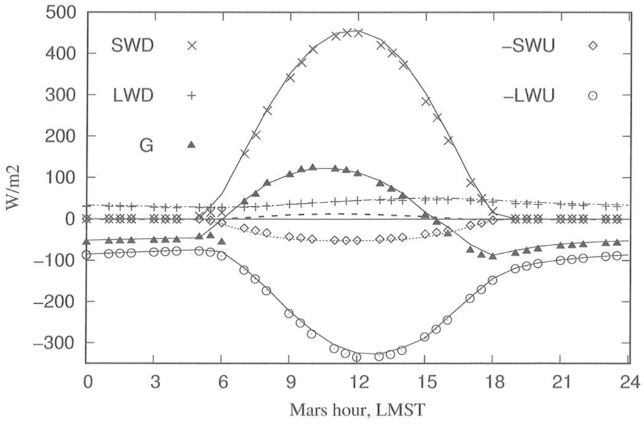

Figure 10. As Figure 3, but for sol 189. The SWD sensor is here saturated at 06:00 LMST and hence the observation-based *G* (the radiation balance) is inaccurate at this hour.

We suspect that the small downscan MEDA TIRS field-of-view for sensors of T_g and LWU landed here onto a bedrock-dominated high-*I* spot, and *I* ~ 350 therefore better represents the typical regolith around the rover. This lower value is also supported by THEMIS retrieval for the site. The typical area-averaged constant *I* is hence obtainable by model fits to diurnally observed lander-T_a rather than to the lander-observed T_g. On the other hand the diurnally variable apparent *I*(*h*) from the diagnostic Fourier method can indicate ground heterogeneities in the small TIRS downscan FOV area for any sol where the rover is stationary and its hourly TIRS observations are complete and error-free.

The high-range T_g-period (191–277 K) covered sols 181–199 (L_s 89°–98°) just after the northern summer solstice. Here good simulations of T_g and the SEB fluxes were obtained with a low constant *I* of 290, and again, even better nonbiased simulations for T_g, when using the diagnostic diurnally variable apparent *I*(*h*). The best model fit to observed T_a was obtained instead for a slightly higher *I* of 350. This value of *I* also agrees with the THEMIS estimate at this site, so presumably the small FOV of the T_g device was located here on a sandy low-*I* spot. Consistently, the nocturnal inversion is here slightly stronger in the observations of T_g and T_a than in the model with the slightly higher *I*.

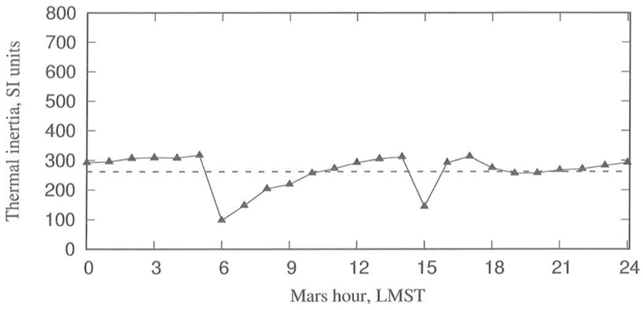

Figure 11. As Figure 4 but for sol 189. Dashed line is the diurnal mean (280).

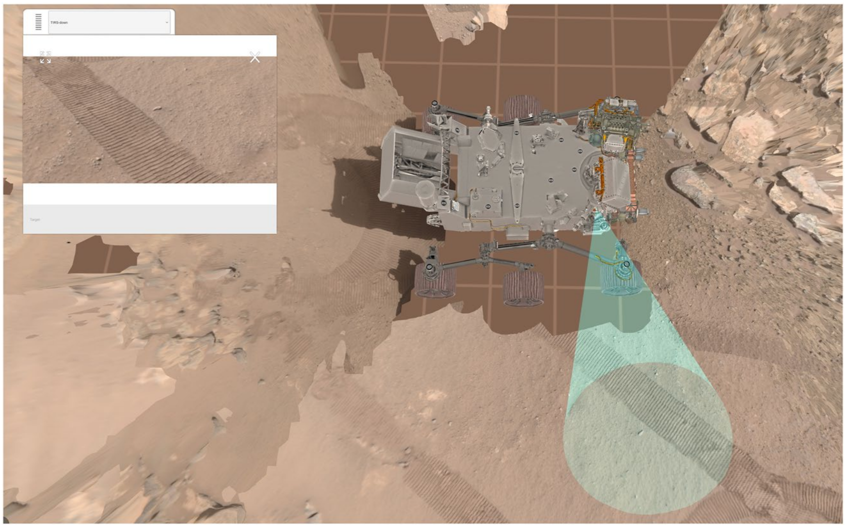

Figure 12. The ground around Perseverance on sol 189. The small field of view (FOV) of the ground-viewing sensor is in the inlet. The FOV consists here of quite smooth sand with a visible rover track, whereas the scenery around the rover appears in general to be sandy regolith with some rocks.

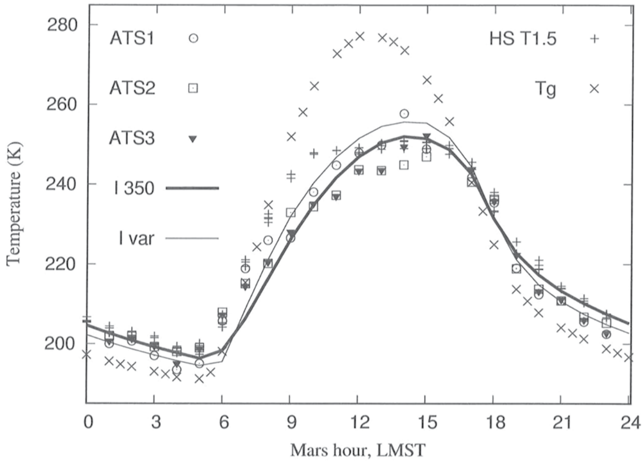

Figure 13. Air temperatures at 1.5 m height for sol 189 from MEDA ATS and HS (symbols), and from SCM simulations (curves) for $I = 350$ and for $I =$ variable, ~290. $I = 350$ provides the better fit with observed air-T. Observed T_g is shown for comparison.

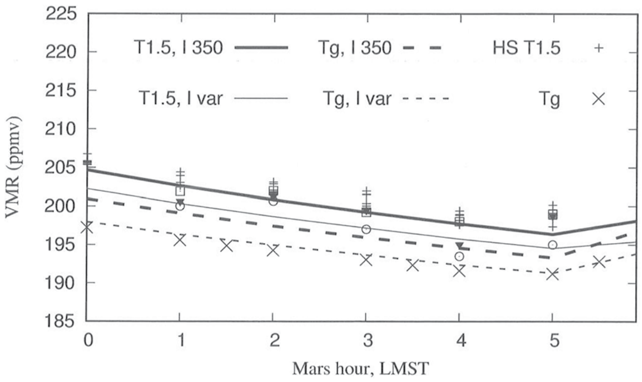

Figure 14. As Figure 8 but for sol 189. Here the observed inversion is stronger than normal, the $I = 350$ simulation again producing a good fit to measured air-T and the var-I simulation to measured T_g.

Data Availability Statement

All Perseverance data used in this study are publicly available via the Planetary Data System (Rodriguez-Manfredi & de la Torre Juarez, 2021). The SCM model results needed for reproducing Figures 3–5, 7–11 and 13–14 of this manuscript are publicly available via the USRA Houston Repository (Savijärvi, Martinez, & Harri, 2022). This repository provides data without restriction or fees. THEMIS retrievals of thermal inertia shown in Figure 2 can be queried and processed using the open-source JMARS (Christensen et al., 2009) and MARSTHERM (Putzig et al., 2013) software.

Acknowledgments
Germán Martínez wants to acknowledge JPL funding from USRA Contract Number 1638782. LPI Contribution No. 2870. LPI is operated by USRA under a cooperative agreement with the Science Mission Directorate of the National Aeronautics and Space Administration. Ari-Matti Harri and Hannu Savijärvi acknowledge the Academy of Finland Grant 310529. Ricardo Hueso, Agustin Sanchez-Laveda and Asier Munguira have greatly helped to process the ATS measurements and Mark Lemmon shared the MastCam-Z opacities.

References

Chen-Chen, H., Perez-Hoyos, S., & Sanchez-Lavega, A. (2021). Assessing multi-stream radiative transfer schemes for the calculation of aerosol radiative forcing in the Martian atmosphere. *Journal of Geophysical Research: Planets*, *126*(10), e2021JE006889. https://doi.org/10.1029/2021JE007889

Christensen, P. R., Engle, E., Anwar, S., Dickenshied, S., Noss, D., Gorelick, N., & Weiss-Malik, M. (2009). JMARS – A planetary GIS. Retrieved from http://adsabs.harvard.edu/abs/2009AGUFMIN22A.06C

Hamilton, V. E., Vasavada, A. R., Sebastian, E., de la Torre Juarez, M., Ramos, M., Armiens, C., et al. (2014). Observations and preliminary science results from the first 100 sols of MSL Rover Environmental Monitoring Station ground temperature sensor measurements at Gale crater. *Journal of Geophysical Research: Planets*, *119*(4), 745–770. https://doi.org/10.1002/2013JE004520

Martínez, G. M., Sebastián, E., Vicente-Retortillo, A., Smith, M. D., Johnson, J. R., Fischer, E., et al. (2023). Surface energy budget, albedo and thermal inertia at Jezero Crater, Mars, as observed from the Mars 2020 MEDA instrument. *Journal of Geophysical Research: Planets*, *128*, e2022JE007537. https://doi.org/10.1029/2022JE007537

Martinez, G. M., Vicente-Retortillo, A., Vasavada, A. R., Newman, C. E., Fischer, E., Renno, N. O., et al. (2021). The surface energy budget at Gale crater during the first 2500 sols of the Mars Science Laboratory mission. *Journal of Geophysical Research: Planets*, *126*(9). https://doi.org/10.1029/2020JE006804

Munguira, A., Hueso, R., Sánchez-Lavega, A., de la Torre-Juarez, M., Martínez, G. M., Newman, C. E., et al. (2023). Near surface atmospheric temperatures at Jezero from Mars 2020 MEDA measurements. *Journal of Geophysical Research: Planets*, *128*, e2022JE007559. https://doi.org/10.1029/2022JE007559

Newman, C. E., Hueso, R., Lemmon, M. T., Munguira, A., Vicente-Retortillo, Á., Apestigue, V., & Guzewich, S. D. (2022). The dynamic atmospheric and aeolian environment of Jezero crater, Mars. *Science Advances*, *8*(21), eabn3783.

Pérez-Izquierdo, J., Sebastián, E., Martínez, G. M., Bravo, A., Ramos, M., & Manfredi, J. A. R. (2018). The Thermal Infrared Sensor (TIRS) of the Mars Environmental Dynamics Analyzer (MEDA) instrument onboard Mars 2020, a general description and performance analysis. *Measurement*, *122*, 432–442. https://doi.org/10.1016/j.measurement.2017.12.004

Polkko, J., Hieta, M., Harri, A.-M., Tamppari, L., Martínez, G., Viúdez-Moreiras, D., et al. (2023). Initial results of the relative humidity observations by MEDA instrument onboard the Mars 2020 Perseverance Rover. *Journal of Geophysical Research: Planets*, *128*, e2022JE007447. https://doi.org/10.1029/2022JE007447

Putzig, N. E., Barratt, E. M., Mellon, M. T., & Michaels, T. I. (2013). MARSTHERM: A web-based System providing thermophysical analysis tools for Mars research. In *AGU Fall Meeting*. Abstract P43C-2023.

Putzig, N. E., & Mellon, M. T. (2007). Thermal behavior of horizontally mixed surfaces on Mars. *Icarus*, *191*(1), 52–67. https://doi.org/10.1016/j.icarus.2007.03.022

Rodriguez-Manfredi, J. A., & de la Torre Juarez, M. (2021). Mars 2020 Perseverance rover Mars environmental Dynamics analyzer (MEDA) experiment data record (EDR) and reduced data record (RDR) data products archive bundle. *PDS Atmospheres Node*. https://doi.org/10.17189/1522849

Rodriguez-Manfredi, J. A., de la Torre Juarez, M., Alonso, A., Apestigue, V., Arruego, I., Atlenza, T., et al. (2021). The Mars Environmental Dynamics Analyzer, MEDA. A suite of environmental sensors for the Mars 2020 mission. *Space Science Reviews*, *217*, 48. https://doi.org/10.1007/s11214-021-00816-9

Savijärvi, H., Crisp, D., & Harri, A. M. (2005). Effects of CO_2 and dust on present-day solar radiation and climate in Mars. *Quarterly Journal of the Royal Meteorological Society*, *131*(611), 2907–2922. https://doi.org/10.1256/qj.04.09

Savijärvi, H., Harri, A.-M., & Kemppinen, O. (2016). The diurnal water cycle at curiosity: Role of exchange with the regolith. *Icarus*, *265*, 63–69. https://doi.org/10.1016/j.icarus.2015.10.008

Savijärvi, H., & Määttänen, A. (2010). Boundary-layer simulations for the Mars Phoenix lander site. *Quarterly Journal of the Royal Meteorological Society*, *136*(651), 1497–1505. https://doi.org/10.1002/qj.650

Savijärvi, H., Martinez, G., Harri, A. M., & Paton, M. (2020). Curiosity observations and column model integrations for a Martian global dust event. *Icarus*, *337*, 113515. https://doi.org/10.1016/j.icarus.2019.113515

Savijärvi, H., Martinez, G. M., & Harri, A.-M. (2022). SCM dataset for manuscript "Surface energy fluxes and temperatures at Jezero crater, Mars. Retrieved from https://repository.hou.usra.edu/handle/20.500.11753/1838

Savijärvi, H., Martinez, G. M., Vicente-Retortillo, A., & Harri, A. M. (2022). Surface energy budget at Curiosity through observations and column modeling. *Icarus*, *376*, 114900. https://doi.org/10.1016/j.icarus.2022.114900

Sebastian, E., Martinez, G. M., Ramos, M., Hanschke, F., Ferrandiz, R., Fernandez, M., & Rodriguez-Manfredi, J. A. (2020). Radiometric and angular calibration tests for the MEDA-TIRS radiometer onboard NASA's Mars 2020 mission. *Measurement*, *164*, 107968. https://doi.org/10.1016/j.measurement.2020.107968

Sebastian, E., Martinez, G. M., Ramos, M., Perez-Grande, I., Sobrado, J., & Rodriguez-Manfredi, J. A. (2021). Thermal calibration of the MEDA-TIRS radiometer onboard NASA's Perseverance rover. *Acta Astronautica*, *182*, 144–159. https://doi.org/10.1016/j.actaastro.2021.02.006

Vasavada, A. R., Piqueux, S., Lewis, K. W., Lemmon, M. T., & Smith, M. D. (2017). Thermophysical properties along Curiosity's traverse in Gale crater, Mars, derived from the REMS ground temperature sensor. *Icarus*, *284*, 372–386. https://doi.org/10.1016/j.icarus.2016.11.035